Substrate Effects on Remote Optical Control of Pt Nanoparticle Driven Olefin Hydrogenation

Maichong Xie, Joseph M. Slocik, Patrick B. Dennis, and Marc R. Knecht, **

- 1. Department of Chemistry, University of Miami, Coral Gables, Florida 33146, USA;
- Materials and Manufacturing Directorate, Air Force Research Laboratory, Dayton,
 Ohio 45433, USA
- 3. Dr. J.T. Macdonald Foundation Biomedical Nanotechnology Institute, University of Miami, Miami, Florida 33136, USA

To whom correspondence should be addressed: MRK – knecht@miami.edu

ABSTRACT

Bio-inspired approaches for materials synthesis and application are emerging as potentially

sustainable approaches to achieve functional structures with selectively controlled

properties (e.g., turn on catalysis). An attractive avenue to allow for selective functionality

is optical stimulation; however, the ability to make nanomaterials light responsive for many

applications remains challenging. One approach is to incorporate photoswitches into the

surface adsorbed ligands which can stimulate a surface structural change that could have

implications on the catalytic reactivity driven by the underlying metallic nanoparticle

component. Herein were demonstrate the ability to drive optical switching of surface

ligand overlayer structures on peptide-capped Pt nanoparticles. To this end, incorporation

of an azobenzene unit into the surface-adsorbed peptide allows for the ability to optical

reconfigure the ligand overlayer structure. This change results in direct manipulation of

the catalytic properties of the Pt materials for olefin hydrogenation, which demonstrated

changes in reactivity not only between different reagents, but also between the different

ligand structures. Such results present information which could be used in the design of

ligand interface structures to trigger specific reactivity control for a variety of reactions and

materials for sustainable catalysis.

KEYWORDS: nanoparticles, peptides, photoswitching, hydrogenation, catalysis

2

INTRODUCTION

Metallic nanoparticles (NPs) are attractive materials for chemical transformations owing to their enhanced surface-to-volume ratio, colloidal stability, and general catalytic reactivity. 1-3 Among them, Pt NPs have garnered significant attention, demonstrating compelling reactivity for reactions including olefin hydrogenation, oxygen reduction, etc.⁴⁻⁷ A variety of synthetic methods have been developed for the production of Pt nanoparticles, which can be energy consuming, require inert environments, or use surfactants and/or organic solvents, thus lowering the sustainability of the synthetic approach.⁸⁻¹¹ Furthermore, once prepared, colloidally dispersed Pt NPs are commonly protected with ligands on the metallic surface, 12-14 thus blocking potential active sites and, as a result, lowering the total possible catalytic reactivity. While these ligands do affect the reactivity, harnessing this effect of blocking active sites could prove to be an opportunity to control the reactivity if the ligands can be programmed to be responsive and expose the active site on demand. Such capabilities remain challenging for two reasons: 1. Ligands are commonly covalently locked in a specific location and 2. Integration of responsivity for structural changes into simple organic ligands remains challenging.

As an alternative to conventional chemical-based NP syntheses, peptide-driven approaches have emerged that could prove to be sustainable strategies for nanomaterial production. ¹⁵⁻¹⁸ These approaches exploit the material specific binding between the peptide and NP surface under ambient conditions (*e.g.*, room temperature and aqueous solvents). A large number of peptides have been identified with affinity for a variety of different inorganic (Au, Ag, Pd, Pt,

CdS, ZnS, etc.)¹⁷ and two dimensional (graphene, *h*-BN, MoS₂, etc.) materials¹⁸ where these biomolecules interact with the material surface through a series of non-covalent interactions at the individual residues. While the localized, individual binding of the residues is relatively weak, the collective binding strength of the peptide is quite strong. Once these materials have been prepared, they have been used for a variety of catalytic applications, including C-C coupling (Stille and Suzuki coupling),¹⁹⁻²² olefin hydrogenation,^{23, 24} nitro-group reduction,²⁵⁻²⁷ electrocatalysis,²⁸⁻³⁰ etc. In general, the reactivity for these peptide-capped materials is achieved under biologically-friendly conditions, making them intriguing structures to access sustainable-based catalysis.

Peptide-driven Pt NP production has been explored,³¹⁻³³ including the production of non-spherical, shaped NPs;³⁴⁻³⁶ however, little information is known concerning their catalytic reactivity for non-electrocatalytic reactions (*e.g.*, olefin hydrogenation). For instance, we have recently reported the use of the AuBP2 (WALRRSIRRQSY) and AgBP1 (TGIFKSARAMRN) peptides to prepare Pt NPs,³³ where noticeable differences in their reactivity for the hydrogenation of allyl alcohol were observed. To this end, enhanced turnover frequency (TOF) values were observed for the AuBP2-capped Pt materials over the NPs capped with the AgBP1 peptide. This suggests that differences in reactivity could be achieved based upon variations in the biomolecular overlayer on the NP surface. Should the ability to reconfigure the biological overlayer structure on a single particle be achieved, changes in the catalytic activity from a single particle could be realized, potentially allowing for selective reaction control.

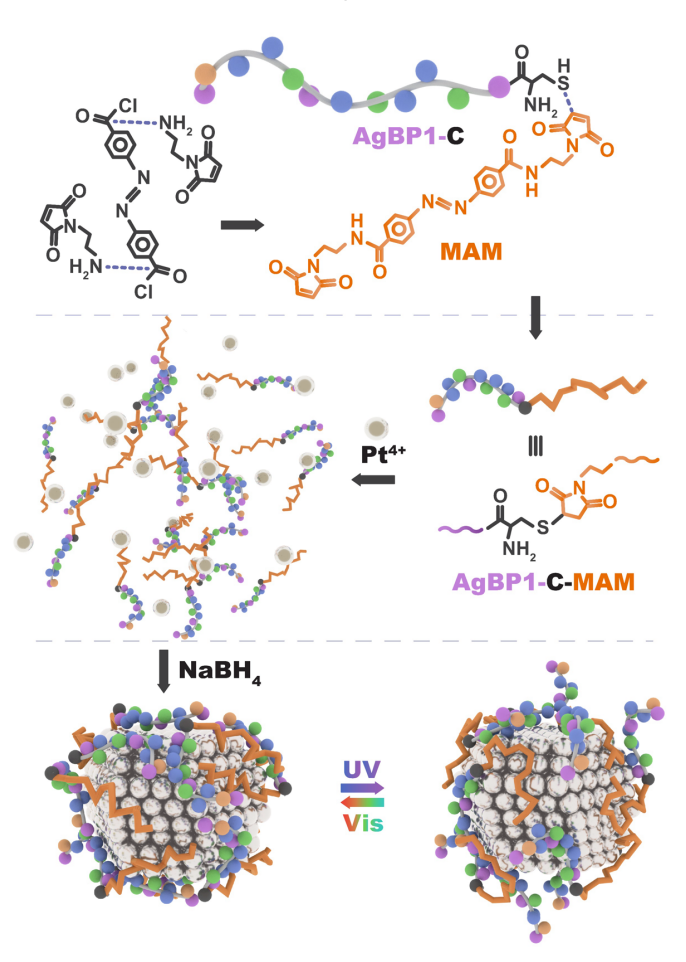
While the binding of the peptides to the metallic surface is generally strong enough to

stabilize the NP, it exploits weak, non-covalent interactions of the amino acid residues. Recent studies have exploited this unique binding modality to achieve light-stimulated reconfiguration of the peptide structure in the surface adsorbed state.³⁷⁻⁴⁰ For this, an azobenzene photoswitch was site-specifically coupled into the peptide. Once the photoswitch/peptide bioconjugate was adsorbed to the NP surface, reversible changes in the biomolecular overlayer can subsequently be achieved via photoswitching of the azobenzene moiety. These changes have been confirmed computationally and spectroscopically, 40, 41 which can be exploited to modulate the catalytic properties of the materials. For instance, varied reactivity for the reduction of 4-nitrophenol to 4-aminophenol was observed for peptide-capped Au NPs with the photoswitch in either the cis or trans configurations.^{25, 42} In this case, the effect was noted to be controlled via changes in the activation energy or the pre-exponential factor of the reaction as dictated by the specific NP/peptide combination.^{25, 41, 42} Subsequent research has demonstrated further understanding of this photoswitch effect on catalysis as a function of peptide sequence, photoswitch position, bioligand heterogeneity, and NP inorganic composition;^{38, 40, 42, 43} however, such effects have only been observed for one single reaction: 4-nitrophenol reduction. No significant understanding of the specific catalytic reaction on photoswitchable catalysis has been considered, which is highly important to understanding such effects on controlling the catalytic properties of inorganic NPs.

Herein, the production of peptide-capped Pt NPs with photoswitchable bioligand interfaces is demonstrated, which were exploited for surface structure-modulated olefin hydrogenation (Scheme 1). This study expands not only the composition of inorganic NPs with photoswitchable interfaces, but also the catalytic process to explore the effects photoswitchable

interfaces on new reactions. For this, the AgBP1 peptide was exploited, which has been shown to have significant affinity for Pt ($\Delta G = -34.6$ \pm 1.2 kJ/mol).³³ To make the peptide light-responsive, azobenzene photoswitch with two terminal maleimides (termed MAM) was siteselectively coupled into the peptide at a cysteine residue incorporated at the C-terminus (bioconjugate termed AgBP1C-MAM – Scheme 1). Using this biological construct, peptide-

Scheme 1. Synthesis of the AgBP1C-MAM peptide-capped Pt NPs and the photoswitching process.



capped Pt NPs were prepared. The materials were fully characterized and the photoswitching capability of the peptides on the metal surface was confirmed. Using these new materials, olefin hydrogenation in water was processed employing a variety of substrates. Remarkably, changes in reactivity as a function of the peptide *cis/trans* configuration were noted for several of the different olefins studied; however, not all of the substrates demonstrated differences in reactivity. These results demonstrate that remotely responsive peptides could be exploited to control NP olefin hydrogenation; however, substrate structure is a key criterion for controlling this reactivity.

EXPERIMENTAL SECTION

dichloride

and

N-(2-aminoethyl)maleimide

Azobenzene-4,4'-dicarbonyl

Materials.

hydrochloride were purchased from Tokyo Chemical Industry (TCI) and stored in glove box under Ar gas. Dichloromethane (DCM) was purchased from Macron Fine Chemicals. Triethylamine (TEA) and N,N-dimethylformamide (DMF) were ordered from EMD Millipore. Diethyl ether and HCl (36.5%-38%) were ordered from VWR BDH chemicals. H₂PtCl₆ was purchased from STREM chemicals and stored at -20 °C under Ar. NaBH₄ was acquired from Beantown Chemical. The AgBP1C peptide was purchased from GenScript and stored at -80 °C. Antifoam SE-15, allyl alcohol, 4-penten-1-ol, 3-buten-2-ol, 1-penten-3-ol, 2-methyl-3-buten-3-ol, and 1,4-pentadien-3-ol were obtained from Sigma-Aldrich, while 3-buten-1-ol was obtained from Fluka Supply Solutions. All reagents were used as received without additional treatment and all aqueous-based experiments were performed with Milli-Q water (18 m Ω ·cm). MAM Photoswitch Synthesis. The MAM photoswitch was synthesized following published protocols with minor modifications.^{38, 40} To this end, 0.1 mmol azobenzene-4,4'-dicarbonyl dichloride was dissolved in 5 mL of DCM, while 0.35 mmol N-(2-aminoethyl)maleimide hydrochloride was dissolved in a mixture of 5 mL of DCM and 0.5 mL TEA in a separate container. The maleimide solution was then added drop-wise into the azobenzene solution on

evaporator to generate an orange solid. This sample was then washed with 20 mL of 0.1 M HCl.

an ice bath under continuous N₂ flow. Once the addition was complete, the mixture was stirred

for 2 days at room temperature. Next, the solution was evaporated to dryness using a rotary

Coupling of MAM and peptide. The coupling of the MAM unit with the AgBP1C peptide to

generate AgBP1C-MAM was accomplished using standard methods with slight variations.^{38, 40} For this, 0.015 mmol AgBP1C and 0.12 mmol MAM (AgBP1C: MAM = 1:8) were dissolved in separate volumes of 5 mL of DMF to generate two solutions. Once prepared, the AgBP1C solution was slowly dripped into the MAM solution, initiating the coupling reaction under steady stirring overnight. When complete, the solution was precipitated with ethyl ether (40 mL), where the newly generated solid was separated via centrifugation, dried, and then redissolved in water. The compound was finally confirmed by MALDI-TOF mass spectrometry.

Synthesis of Peptide-capped Pt NPs. Standard synthesis procedures were followed to prepare the peptide-capped Pt NPs. 33 First, 400 μL of 1 mM aqueous AgBP1C-MAM was diluted with 1576 μL of water. Next, 4 μL of aqueous 100 mM H₂PtCl₆ was added to the system, which was allowed to stir for 15 min. Finally, 20 μL of freshly prepared, aqueous 100 mM NaBH₄ was slowly introduced into the system with gentle shaking. The NPs were allowed to reduce overnight prior to further analysis.

Characterization. UV-vis analysis was conducted with an Agilent 8453 spectrophotometer employing 2 mm quartz cuvettes. Circular dichroism (CD) analysis was performed using a Chirascan V100 CD spectrometer (Applied Photophysics) with 2 mm quartz cuvettes. Fourier transform infrared (FT-IR) spectroscopy was completed using a PerkinElmer Frontier spectrometer on a solution phase sample. Transmission electron microscopy (TEM) samples were prepared by dropping 5 μ L of the synthesized Pt NP solution onto a carbon-coated copper TEM grid, which was then dried in a desiccator for at least 2 h. TEM images were taken using a Tecnai F30 instrument (FEI) with an Octane Elite T55 detector operating at 300 kV. For both

samples, >150 individual NPs were measured to identify the average particle size. Photoinduced-switching of the azobenzene moiety was accessed using published methods.⁴⁰ To this end, the *cis* confirmation of the sample was achieved by exposing the NPs to a 365 nm UV lamp for 30 min. The isomerization of the azobenzene group was verified via UV-vis with the 330 nm peak intensity change.⁴⁴

Catalytic Hydrogenation Reactions. All olefin hydrogenation reactions were carried out using an established method, with minor modifications for the *cis* catalyst form. ⁴⁵ Briefly, 750 μL of 0.2 mM AgBP1C-MAM capped Pt NPs (based upon the total Pt concentration) in the *trans* conformation and 20 μL of antifoam SE-15 were diluted to 25 mL with H₂O in a three-neck round-bottom flask. Note that for the *cis* system, the flask was fully covered by a black blanket and a 365 nm UV lamp illuminated the reaction under the blanket throughout the reaction. The solution was then bubbled with H₂ for 15 min at a flow rate of ~0.5 L/min while stirring at room temperature. Upon completion, 25 mL of an aqueous 10 mM olefinic alcohol solution was quickly injected into the flask to initiate the reaction. During the 1 h reaction, 1 mL aliquots were removed from the system at selected times and quantified via gas chromatography (GC). ⁴⁵ To calculate TOF values, fitting of the analysis from 10-60 min of reaction was employed.

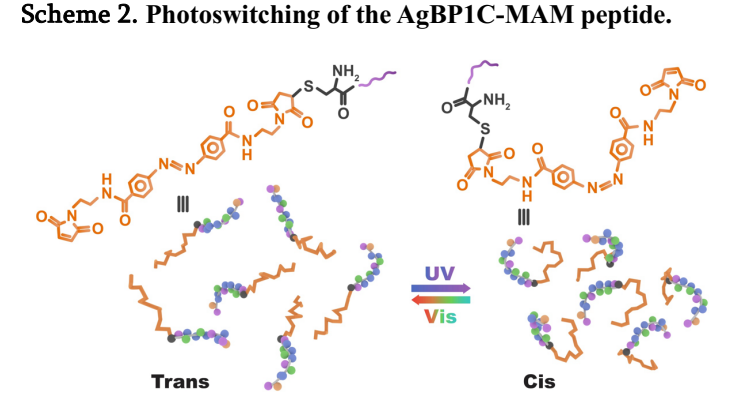
RESULTS AND DISCUSSION

The production of the AgBP1C-MAM photoswitchable peptide was achieved using previously described methods.⁴⁰ This approach relies upon biorthogonal coupling methods that site-

Specifically incorporates the MAM-based photoswitch at the exposed cysteine thiol group. Once the bioconjugate was confirmed via mass spectrometry, it was exploited for production of peptide-capped Pt NPs (Scheme 1). For this, reduction of Pt⁴⁺ ions in the presence of the peptide using NaBH₄ was used to fabricate the materials. Pt⁴⁺ was employed over Pt²⁺ as the lower oxidation state metal ion resulted in the undesired formation of a milky white precipitate after reduction. Using the Pt⁴⁺-based method, the formation of a clear yellow-brown solution was achieved after reduction, suggestive of Pt NP formation. The NPs are prepared with the photoswitch in the *trans* configuration; however, optical irradiation of the molecule facilitates

isomerization of the MAM unit to the

cis conformation (Scheme 2). As shown previously for Au NPs,⁴⁰ this isomerization process results in a significant structural change of the



biomolecule along the peptide backbone, resulting in a shift in the biomolecular overlayer structure between two different configurations, which is referred to as the *trans* and *cis* configuration based upon the isomerization state of the photoswitch.

To monitor NP synthesis, UV-vis analysis was exploited. Figure 1a presents the UV-vis spectra for each step of the reaction to prepare the Pt materials. The green spectrum was obtained from the AgBP1C-MAM alone in solution prior to addition of Pt⁴⁺. In this sample, a strong absorption peak at 330 nm was observed, arising from the $\pi \rightarrow \pi^*$ transition of the azobenzene unit.⁴⁴ After the introduction of one equivalent of Pt⁴⁺ to the peptide (blue spectrum), a new peak 262 nm was observed, which correlated to the Pt-Cl ligand to metal

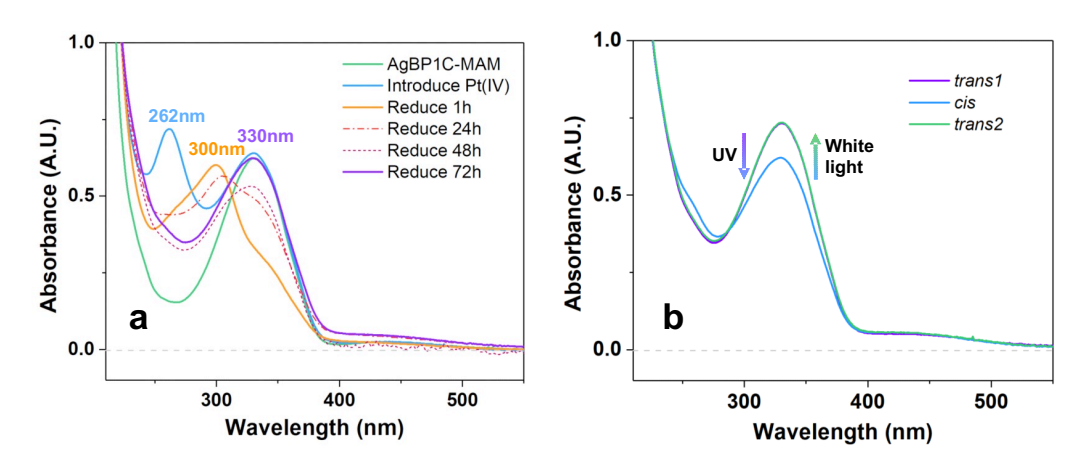


Figure 1. UV-vis analysis of peptide-capped Pt NP synthesis. Part (a) presents the analysis for material synthesis, while part (b) displays the photoswitching analysis of the NPs.

charge transfer band (LMCT).⁴⁶ It is interesting to note that no specific LMCT arising from the complexation of the Pt⁴⁺ to the peptide was observed prior to reduction. The system was subsequently reduced with NaBH₄ and spectroscopically analyzed 1 h post reduction (orange spectrum). At this time point, the Pt-Cl LMCT band was substantially diminished with only a minor shoulder remaining, replaced by a new absorbance at 300 nm. Interestingly, the $\pi \rightarrow \pi^*$ transition of the azobenzene of the peptide was also significantly diminished; however, a notable shoulder at 330 nm remained in the spectrum. The sample was continuously analyzed post reduction, which demonstrated a gradual red shift in the 300 nm absorbance. After 72 h, a restoration of the $\pi \rightarrow \pi^*$ absorbance at 330 nm was noted, which demonstrated an intensity similar to that observed with the free peptide in solution. In addition, an increase in absorbance was noted between 400-500 nm after reduction, consistent with the production of Pt NPs.⁴⁷

Once the Pt NPs were prepared, the isomerization capabilities of the surface adsorbed peptides were examined. For this study, the peptides were switched from the *trans* conformation to the *cis* via irradiation of the sample with UV light from a handheld lamp, while *cis* to *trans* reverse switching was achieved via white light irradiation. To monitor the switching

process, UV-vis analysis of the $\pi\to\pi^*$ absorbance at 330 nm was employed. For this, *trans* to *cis* switching results in diminished absorptivity; however, switching back to the *trans* conformation should result in increased absorptivity. He figure 1b presents this analysis for the peptide-capped Pt NPs. Prior to switching, the sample demonstrated a strong absorbance at 330 nm, as anticipated, which upon UV irradiation resulted in a significant decrease in the absorbance. This decrease confirmed the *trans* to *cis* switching process. Upon irradiation of the sample with white light, increased absorptivity was observed at 330 nm, consistent with the restoration of the *trans* conformation of the peptide, as anticipated. From this comparison, it is clear that *trans* to *cis* switching is occurring under UV irradiation; however, it is likely only a portion of the biomolecules are photoisomerizing. While quantification of the number of photoswitching molecules cannot be determined, based upon the restoration of the 330 nm peak

during visible light irradiation, it can be determined that quantitative cis to trans switching is achieved to return the molecules back to the original state.

To further characterize
the AgBP1C-MAM-capped Pt
NPs, TEM analysis was
performed for two different

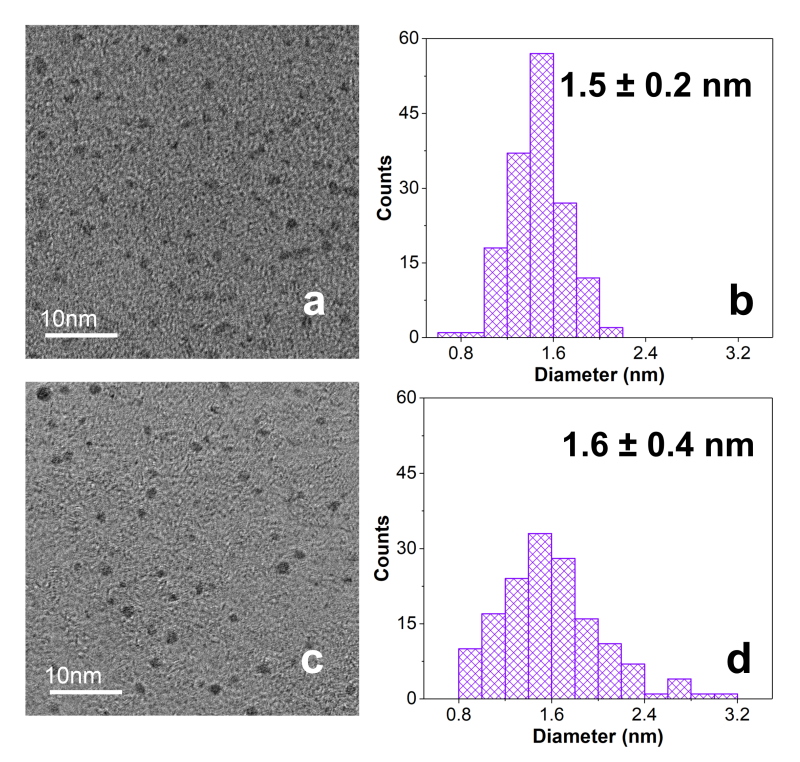


Figure 2. TEM analysis of the AgBP1C-MAM capped Pt NPs. Part (a) presents an image of the NPs 24 h post reduction where part (b) displays the particle size histogram. Parts (c and d) present the same analysis, but after 5 days post reduction.

time points based upon the amount of time the sample was allowed to reduce with NaBH₄ (Figure 2). This study was necessitated by the changes in the UV-vis band structure for the sample after reduction that did not demonstrate restoration of the $\pi\to\pi^*$ absorbance until three days after NaBH₄ addition. Such effects could arise from changes in the NP structure, which was analyzed by TEM. Figure 2a presents the TEM image of the materials 24 h after reduction, which demonstrated an average size of 1.5 \pm 0.2 nm (Figure 2b). When NPs from the same sample were subsequently analyzed five days after NaBH₄ addition, materials of nearly the exact same size were observed (1.6 \pm 0.4 nm – Figure 2c and d). This suggests that the NPs are generally fully formed after 24 h of reduction; however, changes to other components in the system are likely present to affect the optical absorption of the sample.

In addition to UV-vis and TEM, additional characterization of the peptide-capped Pt NPs using CD and FT-IR spectroscopies was performed. Figure 3a presents the CD spectra of the materials throughout the NP synthesis reaction demonstrating an observable structural change to the peptides. In this regard, a clear shift in the feature at 190 nm from the peptide before metal ion reduction (green spectrum) to the NPs 3 days post reduction (purple spectrum)

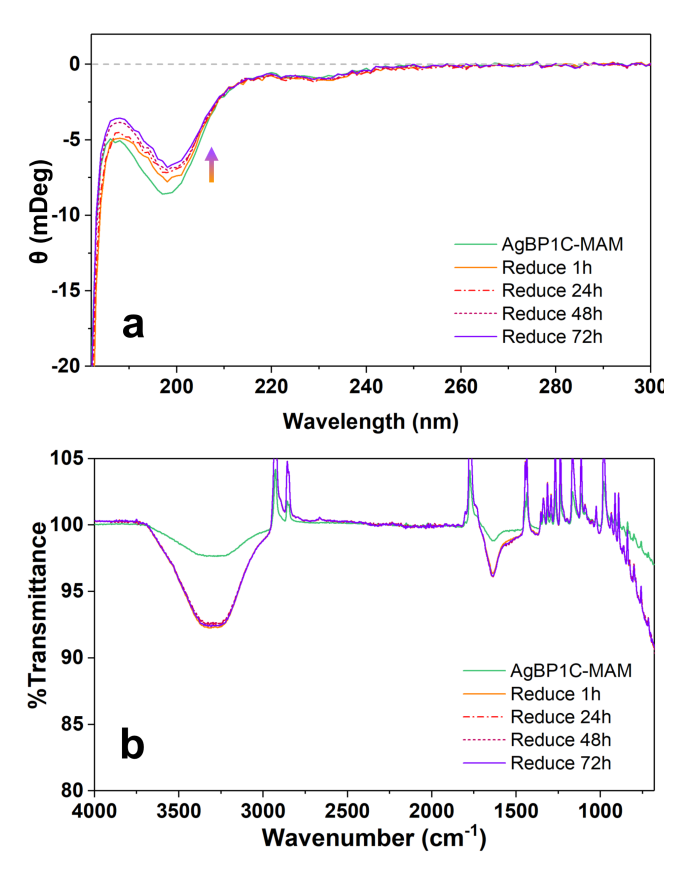


Figure 3. Part (a) CD and part (b) FT-IR analysis of the synthesis of the peptide-capped Pt NPs at the indicated time points.

was evident. Such results are consistent with the UV-vis studies that demonstrated restoration of the $\pi-\pi^*$ azobenzene absorbance after this time period. The CD studies corroborate structural changes throughout these 3 days within the biomolecules on the NP surface. In addition, the interaction between AgBP1C-MAM and the Pt metal surface was also evident through FT-IR analysis (Figure 3b). To this end, the pure AgBP1C-MAM peptide shows characteristic peaks at 3300 (N-H stretching) and 1640 cm⁻¹ (associated with the amide I peak of the peptide backbone). After NP formation, the same peaks were observed, as well as a slight shoulder absorbance at 1530 cm⁻¹ associated with the Amide II absorbance. For the NPs, no significant shift in the FT-IR spectrum was noted as a function of time. This suggests that while changes in peptide secondary structure were noted (as observed via CD and UV-vis), these changes did not significantly affect the FT-IR spectrum of the peptides.

With confirmation of the changes in the biomolecular overlayer structures, variations in the catalytic properties of the materials were explored for olefin hydrogenation (Figure 4). The reaction requires an interaction between the substrate (olefin) and the catalytic surface (Pt), where changes in the peptide surface orientation could have significant impacts on the overall reactivity. Figure 4a specifically shows the reaction process using allyl alcohol as the olefinic substrate. It is important to note that isomerization of the substrate is possible, thus generating propional dehyde. For this reaction, a sufficient volume of the Pt NPs was added to reach a Pt metal concentration of 0.2 mM in the mixture. Once the solution was prepared, it was bubbled with H₂ gas for 15 min, after which the allyl alcohol solution was introduced. To monitor the reaction progress, a series of 1 mL aliquots was extracted from the solution and quantified by

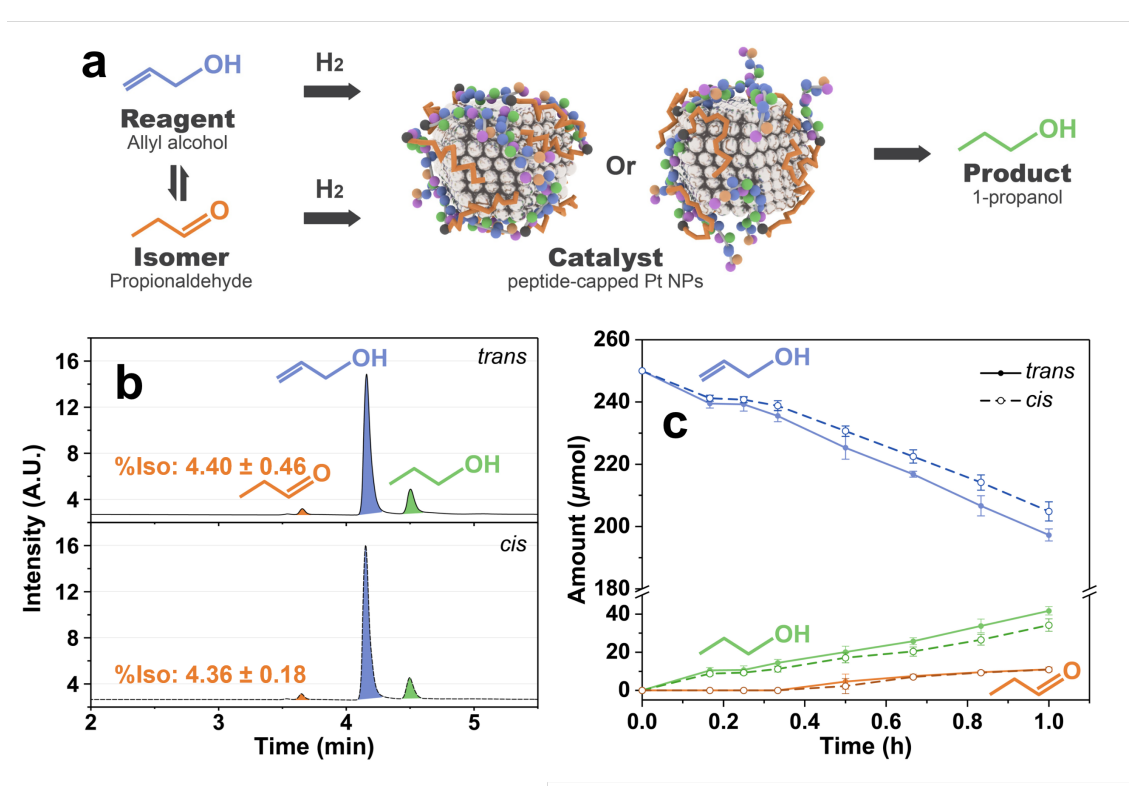


Figure 4. Catalytic hydrogenation analysis of the AgBP1C-MAM-capped Pt NPs with allyl alcohol. Part (a) presents the scheme of the reaction. Part (b) demonstrates the GC analysis of the reaction after 60 min with the peptide in the *trans* (top) and *cis* (bottom) configuration Part (c) displays the reaction progress for both the *trans* and *cis*-based Pt NPs.

GC.^{33, 45} For the reactions using the NPs with the surface adsorbed peptides in the *cis* configuration, the materials in solution were irradiated with a UV lamp for 30 min prior to the reaction. In addition, during the hydrogenation process, the sample was covered to avoid ambient light exposure and continuously irradiated with UV light, thus ensuring that the peptides remained in the *cis* conformation throughout the catalytic process. It is important to note that since the reaction is not photocatalytically-driven, the UV light does not affect the catalytic reaction.

To quantify each aliquot, GC-based sample analysis was used. Figure 4b presents the GC analysis of a sample aliquot for the hydrogenation of allyl alcohol after 60 min of reaction. For this analysis, when the reaction was processed with the peptides in either the *trans* or *cis*

configuration, three specific components were identified in the reaction mixture: 1. allyl alcohol substrate, 2. 1-propanol product, and 3. propionaldehyde isomer. This indicates that the Pt NPs were reactive for the catalytic process in both configurations; however, changes in the level of reactivity, as measured by the TOF value, are possible based upon the isomerization state of the surface adsorbed peptides. Figure 4c presents a comparison of the concentration of the three components in the reaction mixture as a function of time. In addition, the analysis presents the reactivity of the NPs in both the *cis* and *trans* conformation. In general, the amount of reagent decreased concomitant with an increase in the amount of the final hydrogenated product throughout the reaction. That said, it is clear that more catalytic turnover was observed from the Pt NPs with the peptide in the *trans* configuration as more product was generated from this system. A small amount of the isomer was also evident throughout the reaction.

Using the data of Figure 4c, TOF values can be determined for the peptide-capped Pt NPs with the photoswitch in the two different conformations. For the NPs with the peptides in the *trans* configuration, a TOF value of 254.6 ± 14.2 mol product/(mol metal \times h) was quantified, which decreased to 203.1 ± 18.8 mol product/(mol metal \times h) for the same NPs with the peptides in the *cis* configuration. Please note that these values represent the average TOF \pm one standard deviation achieved from triplicate catalytic reactions. This indicates that the materials were generally more reactive for the *trans*-based system, suggesting that changes in the ligand overlayer structure on the NP surface has a significant effect on the reactivity of the materials. This may arise from changes in the presentation or accessibility to the catalytic metal surface, thus altering the overall NP reactivity.

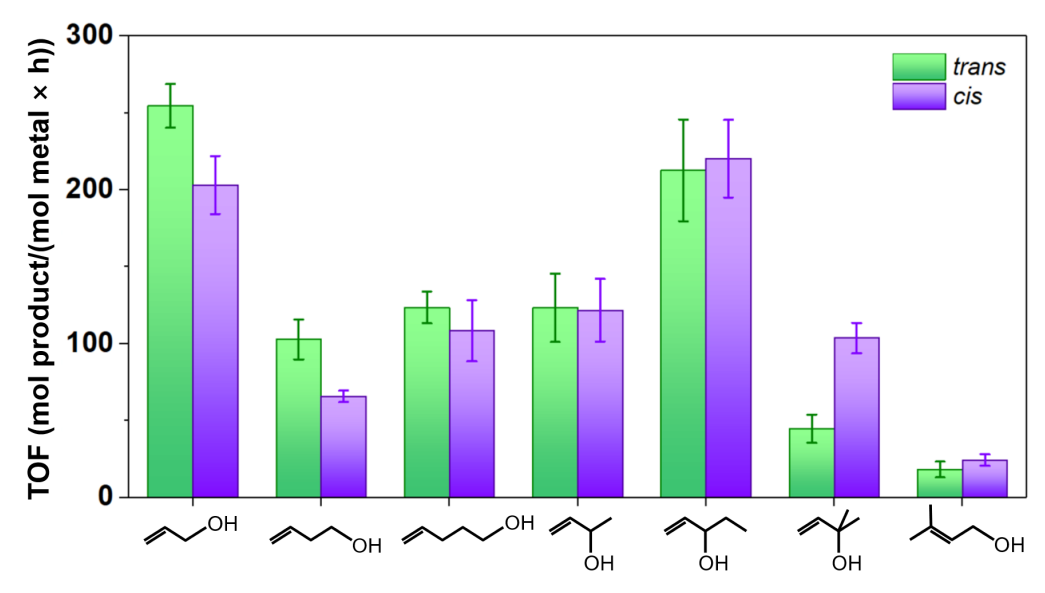


Figure 5. Catalytic hydrogenation analysis of peptide-capped Pt NPs with indicated substrate.

Expanding the scope of reaction substrates to more complex species was also explored to understand such effects on photoswitchable olefin hydrogenation (Figure 5). To this end, the effect of substrate size was examined by changing the length of the carbon chain using 3-buten-1-ol and 4-penten-1-ol as the substrate. In this case, the system was still a primary alcohol, as was the original allyl alcohol reactant. For the longer chained species, the TOF values were 102.7 ± 12.9 mol product/(mol metal × h) and 123.6 ± 10.3 mol product/(mol metal × h) for 3-buten-1-ol and 4-penten-1-ol, respectively, for the reaction studied with the peptides in the *trans* configuration. Such values were notably lower than what was observed for the allyl alcohol-based reaction. When the same process was studied using the Pt NPs with the peptides in the *cis* configuration, the TOF values generally decreased, on average, as compared to reaction completed using the particles with the peptides in the *trans* conformation (65.9 \pm 3.7 mol product/(mol metal × h) for 3-buten-1-ol and 108.4 ± 19.9 mol product/(mol metal × h) for 4-penten-1-ol).

To increase the complexity of the substrate, two secondary (3-buten-2-ol and 1-penten-3-

ol) and one tertiary (2-methyl-3-buten-2-ol) alcohols were also examined in the reaction. Interestingly, using the secondary alcohols, no significant effects of the overlayer conformation were observed on the reactivity. For instance, when 3-buten-2-ol was used for the reaction, TOF values of 123.3 ± 22.2 mol product/(mol metal × h) and 121.7 ± 20.4 mol product/(mol metal × h) were noted for the peptides in the *trans* and *cis* confirmation, respectively. Similar effects were noted for the reaction studied using 1-penten-3-ol as the substrate, albeit with a higher overall degree of reactivity (212.7 ± 33.1 mol product/(mol metal × h) and 220.3 ± 25.2 mol product/(mol metal × h) for *trans* and *cis*, respectively). When the reaction was studied using the tertiary alcohol, significant effects of the overlayer conformation were noted. To this end, with the Pt NPs with the peptides in the *trans* conformation, a TOF value of 44.7 ± 9.2 mol product/(mol metal × h) was observed, which substantially increased to 103.6 ± 9.9 mol product/(mol metal × h) with the NPs presenting the *cis* conformation of the peptides.

In addition, to explore the influence of the double bond location, an internal olefinic alcohol, 3-methyl-2-buten-1-ol, was examined. Compared to the terminal olefins, the TOF values for this substrate were relatively small: 18.3 ± 5.1 mol product/(mol metal × h) for the Pt NPs with the peptide in the *trans* configuration and 24.3 ± 3.7 mol product/(mol metal × h)) for the NPs with the *cis*-based peptides. While reactivity was observed, it was significantly lower than for the terminal-based olefins, suggesting that placement of the alkene bond can play a significant effect in the overall reactivity.

Further substrate analysis was conducted using 1,4-pentadien-3-ol as a representative dienol to be explored for multistep catalytic hydrogenation (Figure 6a). Using this substrate, 1-

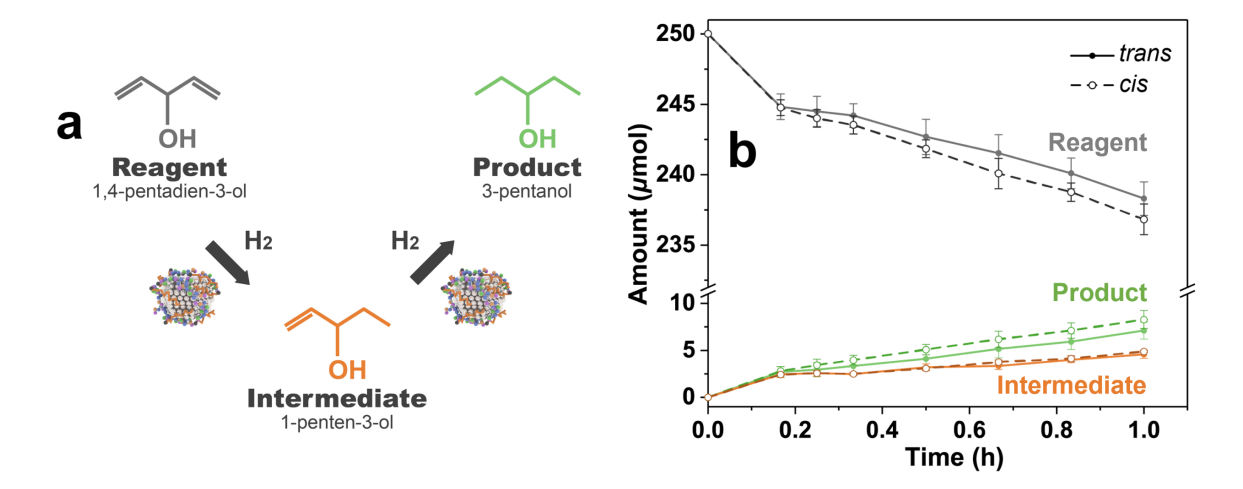


Figure 6. Catalytic hydrogenation analysis of 1,4-pentadien-3-ol employing the AgBP1C-MAM-capped Pt NPs. Part (a) illustrates the scheme of the reaction, while part (b) displays the reaction progress.

penten-3-ol is generated as an intermediated, which is finally converted to 3-pentanol as the product. Using the dienol as the substrate, rapid reagent consumption was noted for the Pt NPs with the peptide in both the *trans* and *cis* conformations, along with simultaneous production of both the intermediate and final product. This suggests that both the dienol reagent and 1-penten-3-ol intermediate were simultaneously reacting on the Pt surface. Throughout the 1 h reaction time frame, the reagent was consumed and the final product concentration increased; however, the rate of final product production was greater than the rate of intermediate generation.

When comparing the reactivity of the peptide-capped Pt NPs with the biomolecules in the *cis* and *trans* configuration, similar reactivity effects were noted; however, faster reactivity was indicated from the particles in the *cis* configuration (Figure 6b). This was evident by a more rapid consumption of the starting materials. To calculate TOF values, consumption of the dienol reagent was employed, which is more reflective of the overall reaction. Furthermore, this avoids the convolution of intermediate production and consumption that would be inherent in

the calculation using the production of the final product. Using this method, the TOF value for the consumption of the dienol for the Pt NPs in the *trans* configuration was 54.4 ± 2.4 mol reagent/(mol metal \times h); however, when using the same NPs with the peptides in the *cis* conformation, the TOF value increased to 63.2 ± 4.2 mol reagent/(mol metal \times h). Such effects indicate that the reactivity for the dienol was sensitive to the biomolecular overlayer structure to control the hydrogenation process.

From the substrate complexity analysis, it is clear that changes in reactivity were noted based upon differences in reagent structure; however, no specific trend could be identified. On average, from the primary alcohols, greater reactivity was noted for the peptides in the *trans* conformation; however, for the tertiary alcohols, notably faster reactivity was observed for the NPs with the *cis* conformation. In addition, when using the secondary alcohol substrates, no difference in reactivity was noted based upon the peptide configuration, yet for the dienol, greater reactivity was observed for the *cis*-based materials over the *trans* NPs. Such effects may arise from a variety of factors including NP structural effects that alter accessibility to the metal surface, substrate solubility, ease of interaction of the olefin with the metal surface, etc. While it is clear that differences in absolute reactivity (*i.e.*, reactivity between different substrates) and, in some cases, reactivity between different peptide conformations were evident, the basis for these differences remains unclear.

CONCLUSIONS

In conclusion, these results demonstrated intriguing new capabilities in the optical control of catalytic reactions. In this regard, Pt NPs capped with peptides containing an integrated photoswitch were prepared that could reversibly change the surface structure of the materials. This variation in overlayer morphology had direct effects on the catalytic reaction, which is highly dependent upon the amount of available metallic surface area to drive the chemical transformation. Interestingly, the reaction and its TOF varied based upon the structure of the olefinic substrate. These changes affected both the overall TOF value and the sensitivity to the surface structure. The materials were also reactive to multistep reactivity for conversion of dienols to fully saturated final products, which was also sensitive to the surface overlayer morphology. Such results are intriguing and demonstrate new reactivity trends for selective catalysts in new reactions. These results could be used to identify new routes for more precise optical control of surface structures and their effects on reactivity.

AUTHOR INFORMATION

Corresponding Author

*MRK – knecht@miami.edu

Author Contributions

This manuscript was written through the contributions of all of the authors. All authors approved the final version of the manuscript.

Notes

The authors declare no competing financial interest.

21

ACKNOWLEDGMENTS

This material is based upon work supported by the National Science Foundation under Grants No. 1903649 and 2203862 (M.R.K.).

References

- (1) Gao, C.; Lyu, F.; Yin, Y. Encapsulated metal nanoparticles for catalysis. *Chem. Rev.* **2020**, *121*, 834-881.
- (2) Li, Z.; Ji, S.; Liu, Y.; Cao, X.; Tian, S.; Chen, Y.; Niu, Z.; Li, Y. Well-defined materials for heterogeneous catalysis: from nanoparticles to isolated single-atom sites. *Chem. Rev.* **2019**, *120*, 623-682.
- (3) Liu, L.; Corma, A. Bimetallic sites for catalysis: from binuclear metal sites to bimetallic nanoclusters and nanoparticles. *Chem. Rev.* **2023**, *123*, 4855-4933.
- (4) Bai, L.; Wang, X.; Chen, Q.; Ye, Y.; Zheng, H.; Guo, J.; Yin, Y.; Gao, C. Explaining the size dependence in platinum-nanoparticle-catalyzed hydrogenation reactions. *Angew. Chem. Int. Ed.* **2016**, *55*, 15656-15661.
- (5) Crooks, R.; Zhao, M. Dendrimer Encapsulated Pt Nanoparticles: Synthesis, Characterization, and Applications to Catalysis. *Adv. Mater.* **1999**, *11*, 217-220.
- (6) Formo, E.; Lee, E.; Campbell, D.; Xia, Y. Functionalization of electrospun TiO2 nanofibers with Pt nanoparticles and nanowires for catalytic applications. *Nano Lett.* **2008**, *8*, 668-672.
- (7) Khan, M. A. R.; Al Mamun, M. S.; Ara, M. H. Review on platinum nanoparticles: Synthesis, characterization, and applications. *Microchem. J.* **2021**, *171*, 106840.
- (8) Chen, A.; Holt-Hindle, P. Platinum-based nanostructured materials: synthesis, properties, and applications. *Chem. Rev.* **2010**, *110*, 3767-3804.
- (9) Eklund, S. E.; Cliffel, D. E. Synthesis and catalytic properties of soluble platinum nanoparticles protected by a thiol monolayer. *Langmuir* **2004**, *20*, 6012-6018.

- (10) Knecht, M. R.; Weir, M. G.; Myers, V. S.; Pyrz, W. D.; Ye, H.; Petkov, V.; Buttrey, D. J.; Frenkel, A. I.; Crooks, R. M. Synthesis and characterization of Pt dendrimer-encapsulated nanoparticles: effect of the template on nanoparticle formation. *Chem. Mater.* **2008**, *20*, 5218-5228.
- (11) Xin, Y.; Nagata, T.; Kato, K.; Shirai, T. Microwave-assisted synthesis of Pt nanoparticles via liquid-phase polyol reaction for catalytic volatile organic compound elimination. *ACS Appl. Nano Mater.* **2022**, *5*, 4305-4315.
- (12) Cremer, P. S.; Somorjai, G. A. Surface science and catalysis of ethylene hydrogenation. *J. Chem. Soc., Faraday Trans.* **1995,** *91,* 3671-3677.
- (13) Luo, L.; Duan, Z.; Li, H.; Kim, J.; Henkelman, G.; Crooks, R. M. Tunability of the adsorbate binding on bimetallic alloy nanoparticles for the optimization of catalytic hydrogenation. *J. Am. Chem. Soc.* **2017**, *139*, 5538-5546.
- (14) Morsbach, E.; Spéder, J.; Arenz, M.; Brauns, E.; Lang, W.; Kunz, S.; Bäumer, M. Stabilizing catalytically active nanoparticles by ligand linking: toward three-dimensional networks with high catalytic surface area. *Langmuir* **2014**, *30*, 5564-5573.
- (15) Mokashi-Punekar, S.; Zhou, Y.; Brooks, S. C.; Rosi, N. L. Construction of chiral, helical nanoparticle superstructures: progress and prospects. *Adv. Mat.* **2020,** *32,* 1905975.
- (16) Tadepalli, S.; Slocik, J. M.; Gupta, M. K.; Naik, R. R.; Singamaneni, S. Bio-optics and bio-inspired optical materials. *Chem. Rev.* **2017**, *117*, 12705-12763.
- (17) Walsh, T. R.; Knecht, M. R. Biointerface structural effects on the properties and applications of bioinspired peptide-based nanomaterials. *Chem. Rev.* **2017**, *117*, 12641-12704. (18) Walsh, T. R.; Knecht, M. R. Biomolecular material recognition in two dimensions: peptide

binding to graphene, h-BN, and MoS2 nanosheets as unique bioconjugates. *Bioconjugate Chem.* **2019,** *30,* 2727-2750.

- (19) Briggs, B. D.; Bedford, N. M.; Seifert, S.; Koerner, H.; Ramezani-Dakhel, H.; Heinz, H.; Naik, R. R.; Frenkel, A. I.; Knecht, M. R. Atomic-scale identification of Pd leaching in nanoparticle catalyzed C–C coupling: effects of particle surface disorder. *Chem. Sci.* **2015**, *6*, 6413-6419.
- (20) Briggs, B. D.; Pekarek, R. T.; Knecht, M. R. Examination of transmetalation pathways and effects in aqueous Suzuki coupling using biomimetic Pd nanocatalysts. *J. Phys. Chem. C* **2014**, *118*, 18543-18553.
- (21) Corulli, C. J.; Groover, E. A.; Attelah, J. D.; Miller, C. B.; Penland, B. B. Rational design of peptides for biomimetic palladium nanoparticle catalysis with Suzuki and Heck coupling in ethanol. *J. Colloid interface Sci.* **2023**, *54*, 100708.
- (22) Pacardo, D. B.; Sethi, M.; Jones, S. E.; Naik, R. R.; Knecht, M. R. Biomimetic synthesis of Pd nanocatalysts for the Stille coupling reaction. *ACS Nano* **2009**, *3*, 1288-1296.
- (23) Bedford, N. M.; Ramezani-Dakhel, H.; Slocik, J. M.; Briggs, B. D.; Ren, Y.; Frenkel, A. I.; Petkov, V.; Heinz, H.; Naik, R. R.; Knecht, M. R. Elucidation of peptide-directed palladium surface structure for biologically tunable nanocatalysts. *ACS Nano* **2015**, *9*, 5082-5092.
- (24) Merrill, N. A.; McKee, E. M.; Merino, K. C.; Drummy, L. F.; Lee, S.; Reinhart, B.; Ren, Y.; Frenkel, A. I.; Naik, R. R.; Bedford, N. M. Identifying the atomic-level effects of metal composition on the structure and catalytic activity of peptide-templated materials. *ACS Nano* **2015**, *9*, 11968-11979.
- (25) Lawrence, R. L.; Scola, B.; Li, Y.; Lim, C.-K.; Liu, Y.; Prasad, P. N.; Swihart, M. T.;

- Knecht, M. R. Remote optically controlled modulation of catalytic properties of nanoparticles through reconfiguration of the inorganic/organic interface. *ACS Nano* **2016**, *10*, 9470-9477.
- (26) Lee, N.; Lee, D.-W.; Lee, S.-M. Gold nanoparticle-stabilized, tyrosine-rich peptide self-assemblies and their catalytic activities in the reduction of 4-nitrophenol. *Biomacromolecules* **2018**, *19*, 4534-4541.
- (27) Li, Y.; Tang, Z.; Prasad, P. N.; Knecht, M. R.; Swihart, M. T. Peptide-mediated synthesis of gold nanoparticles: effects of peptide sequence and nature of binding on physicochemical properties. *Nanoscale* **2014**, *6*, 3165-3172.
- (28) Bedford, N. M.; Showalter, A. R.; Woehl, T. J.; Hughes, Z. E.; Lee, S.; Reinhart, B.; Ertem, S. P.; Coughlin, E. B.; Ren, Y.; Walsh, T. R. Peptide-directed PdAu nanoscale surface segregation: toward controlled bimetallic architecture for catalytic materials. *ACS Nano* **2016**, *10*, 8645-8659.
- (29) Yang, H.; Tang, Z.; Yan, W.; Wang, L.; Wang, Q.; Zhang, Y.; Liu, Z.; Chen, S. Peptide capped Pd nanoparticles for oxygen electroreduction: strong surface effects. *J. Alloys Compd.* **2017,** *702,* 146-152.
- (30) Zhu, E.; Yan, X.; Wang, S.; Xu, M.; Wang, C.; Liu, H.; Huang, J.; Xue, W.; Cai, J.; Heinz, H. Peptide-assisted 2-D assembly toward free-floating ultrathin platinum nanoplates as effective electrocatalysts. *Nano Lett.* **2019**, *19*, 3730-3736.
- (31) Bhandari, R.; Pacardo, D. B.; Bedford, N. M.; Naik, R. R.; Knecht, M. R. Structural control and catalytic reactivity of peptide-templated Pd and Pt nanomaterials for olefin hydrogenation. *J. Phys. Chem. C* **2013**, *117*, 18053-18062.
- (32) Li, Y.; Whyburn, G. P.; Huang, Y. Specific peptide regulated synthesis of ultrasmall

- platinum nanocrystals. J. Am. Chem. Soc. 2009, 131, 15998-15999.
- (33) Xie, M.; Shimogawa, R.; Liu, Y.; Zhang, L.; Foucher, A. C.; Routh, P. K.; Stach, E. A.; Frenkel, A. I.; Knecht, M. R. Biomimetic Control over Bimetallic Nanoparticle Structure and Activity via Peptide Capping Ligand Sequence. *ACS Nano* **2024**, *18*, 3286-3294.
- (34) Chiu, C.-Y.; Li, Y.; Ruan, L.; Ye, X.; Murray, C. B.; Huang, Y. Platinum nanocrystals selectively shaped using facet-specific peptide sequences. *Nat. Chem.* **2011**, *3*, 393-399.
- (35) Forbes, L. M.; Goodwin, A. P.; Cha, J. N. Tunable size and shape control of platinum nanocrystals from a single peptide sequence. *Chem. Mater.* **2010**, *22*, 6524-6528.
- (36) Ruan, L.; Chiu, C.-Y.; Li, Y.; Huang, Y. Synthesis of platinum single-twinned right bipyramid and {111}-bipyramid through targeted control over both nucleation and growth using specific peptides. *Nano Lett.* **2011**, *11*, 3040-3046.
- (37) Lawrence, R. L.; Olagunju, M. O.; Liu, Y.; Mahalingam, K.; Slocik, J. M.; Naik, R. R.; Frenkel, A. I.; Knecht, M. R. Remote controlled optical manipulation of bimetallic nanoparticle catalysts using peptides. *Catal. Sci. Technol.* **2021**, *11*, 2386-2395.
- (38) Xie, M.; Slocik, J. M.; Kelley-Loughnane, N.; Knecht, M. R. Effect of a Mixed Peptide Ligand Layer on Au Nanoparticles for Optical Control of Catalysis. *ACS Appl. Nano Mater.* **2022,** *5*, 9379-9388.
- (39) Palafox-Hernandez, J. P.; Lim, C.-K.; Tang, Z.; Drew, K. L.; Hughes, Z. E.; Li, Y.; Swihart, M. T.; Prasad, P. N.; Knecht, M. R.; Walsh, T. R. Optical actuation of inorganic/organic interfaces: comparing peptide-azobenzene ligand reconfiguration on gold and silver nanoparticles. *ACS Appl. Mater. Interfaces* **2016**, *8*, 1050-1060.
- (40) Tang, Z.; Lim, C.-K.; Palafox-Hernandez, J. P.; Drew, K. L.; Li, Y.; Swihart, M. T.; Prasad,

- P. N.; Walsh, T. R.; Knecht, M. R. Triggering nanoparticle surface ligand rearrangement via external stimuli: light-based actuation of biointerfaces. *Nanoscale* **2015**, *7*, 13638-13645.
- (41) Olagunju, M. O.; Liu, Y.; Frenkel, A. I.; Knecht, M. R. Atomically Resolved Characterization of Optically Driven Ligand Reconfiguration on Nanoparticle Catalyst Surfaces. *ACS Appl. Mater. Interfaces* **2021,** *13*, 44302-44311.
- (42) Lawrence, R. L.; Hughes, Z. E.; Cendan, V. J.; Liu, Y.; Lim, C.-K.; Prasad, P. N.; Swihart, M. T.; Walsh, T. R.; Knecht, M. R. Optical control of nanoparticle catalysis influenced by photoswitch positioning in hybrid peptide capping ligands. *ACS Appl. Mater. Interfaces* **2018**, *10*, 33640-33651.
- (43) Lawrence, R. L.; Cendan, V. J.; Scola, B.; Liu, Y.; Lim, C.-K.; Prasad, P. N.; Swihart, M. T.; Knecht, M. R. Optical Control of Biomimetic Nanoparticle Catalysts Based upon the Metal Component. *J. Phys. Chem. C* **2018**, *122*, 28055-28064.
- (44) Bandara, H. D.; Burdette, S. C. Photoisomerization in different classes of azobenzene. *Chem. Soc. Rev.* **2012**, *41*, 1809-1825.
- (45) Bhattacharjee, S.; Bruening, M. L. Selective hydrogenation of monosubstituted alkenes by Pd nanoparticles embedded in polyelectrolyte films. *Langmuir* **2008**, *24*, 2916-2920.
- (46) Kozyr, E. G.; Njoroge, P. N.; Chapek, S. V.; Shapovalov, V. V.; Skorynina, A. A.; Pnevskaya, A. Y.; Bulgakov, A. N.; Soldatov, A. V.; Pellegrino, F.; Groppo, E. Operando Laboratory X-ray Absorption Spectroscopy and UV–Vis Study of Pt/TiO2 Photocatalysts during Photodeposition and Hydrogen Evolution Reactions. *Catalysts* **2023**, *13*, 414.
- (47) Creighton, J. A.; Eadon, D. G. Ultraviolet–visible absorption spectra of the colloidal metallic elements. *J. Chem. Soc., Faraday Trans.* **1991,** *87,* 3881-3891.

- (48) Ji, Y.; Yang, X.; Ji, Z.; Zhu, L.; Ma, N.; Chen, D.; Jia, X.; Tang, J.; Cao, Y. DFT-calculated IR spectrum amide I, II, and III band contributions of N-methylacetamide fine components. *ACS omega* **2020**, *5*, 8572-8578.
- (49) Singh, B. R., *Basic aspects of the technique and applications of infrared spectroscopy of peptides and proteins*. ACS Publications: **2000**.
- (50) Zaera, F. On the mechanism for the hydrogenation of olefins on transition-metal surfaces: The chemistry of ethylene on Pt (111). *Langmuir* **1996,** *12,* 88-94.

FOR TABLE OF CONTENTS USE ONLY

